JOURNAL OF Applied Polymer SCIENCE

Low Energy Impact Indentation of a Modified Polyethylene Terephtalate by Instrumented Falling Weight

A. B. Martínez, D. Arencón, J. Navas, J. I. Velasco

Centre Català del Plàstic, Dpt. Materials Science and Metallurgy, Universitat Politècnica de Catalunya—BarcelonaTECH, C/Colom, 114, 08222 Terrassa, Spain

Correspondence to: D. Arencón (E-mail: david.arencon@upc.edu)

ABSTRACT: Investigation of the flexed plate impact of polymers requires the study of the local plate reaction during the contact between the hemispherical tip and the specimen. The current work investigates the low energy impact indentation with a hemispherical indenter applied to a polymer sheet with a ductile behavior. The samples were freely supported on a very rigid steel plate and transversely collided by the instrumented dart. The restitution coefficients are calculated, and a lumped mass-spring model based on the Hertz law, which agrees with the experimental contact forces, restitution coefficients, indenter depth of penetration and permanent deformations is developed. This is an indirect method to estimate the Young's modulus at these relatively high strain rates. The influence of the geometrical parameters of the test such as target thickness, drop mass, indenter diameter, along with impact velocity are analyzed. © 2012 Wiley Periodicals, Inc. J. Appl. Polym. Sci. 000: 000–000, 2012

KEYWORDS: impact resistance; indentation; modeling; polyesters

Received 25 July 2010; accepted 27 April 2012; published online
DOI: 10.1002/app.37969

INTRODUCTION

The subject of impact attracts the interest of scientists and engineers from different areas of knowledge. The common goal is to develop theories that can predict the behavior of colliding objects. The impact event involves the motion of the specimen, the motion of the striker, and the local indentation in the contact zone.

In the flexed plate configuration, a falling hemispherical tipped dart collides transversally against plate-shaped specimens simply supported on a metallic ring. The specimen behavior during impact may be separated in two parts: the contact with the falling dart and the plate deflection.

The effect of the local indentation can be studied through the collision of a specimen supported over a very rigid steel plate in the indentation impact tests with the flexed plate configuration, which has a striker with a hardened steel hemispherical head.

Indentation of a halfspace by a spherical indenter is a classic contact problem.[1] However, the impact between a rigid spherical body and a plane surface is a complicated event. It offers the possibility of determining the dynamic hardness and rate-dependent response of the material and is an indirect method of assessing Young's modulus. The main characteristics of the problem are the short duration and the large localized stresses in the vicinity of the contact area. Therefore, plastic deformation is often involved.

The restitution coefficient is a global measure of the energy lost during collision. The kinetic energy loss can be attributed to different forms of energy dissipation such as: frictional losses from the two surfaces sliding, production of sound, energy transformed into internal vibrations, and losses due to material deformation. Because the first four means of energy dissipation are negligible for these conditions, the losses due to material deformation, mainly plastic and some viscoelastic, must be responsible for the energy loss during the impact. If material deformation occurs, then there is a residual impression left in the specimen surface. This coefficient is not an intrinsic material property,[2] but rather it depends on the materials of colliding bodies, their surface geometry, and impact velocity. If there is no energy loss, the systems are conservative, whereas in nonconservative systems energy loss takes place. Almost all real systems are not conservative to greater or lesser degree.

The traditional approach used to measure the dynamic hardness employs a metal ball, which drops onto a massive specimen, in a similar configuration to that used in this impact test. Relatively little work has been done on dynamic indentation

compared to the static counterpart, although the dynamic indentation with spherical indenters has been applied to rubber[3,4] and composite materials.[5,6]

A first step toward understanding the impact indentation with a hemispherical indenter involves the modeling of the system dynamics. The Hertz theory of impact[7] has been applied to predict the indentation force as a function of the time in the conservative mass-spring model.[5] In nonconservative approaches, motion equation is increased with a damping term to reflect dissipation in the contact area, thus allowing us to effectively model the system as a lumped mass-spring model in series[6] or in parallel.[4]

The investigation described below was initiated with several aims. Firstly, the evaluation of the energy loss in the dynamic indentation test, which can be obtained from the restitution coefficient. Secondly, the development of a nonconservative dynamic model which can be successfully adopted for predicting both the restitution coefficient and the indentation force versus time during the impact indentation of the specimen. To check the validity of the model, the influence of several geometric test parameters such as target thickness, indenter mass, and indenter diameter have been studied at different initial velocities.

EXPERIMENTAL PROCEDURE

Material

A commercial grade of a modified poly(ethylene terephthalate) with cyclohexanedimethanol (PETG), *Spectar 14471* from *Eastman Chemical Co.* was selected for this study. This modification improves the melt strength, and suppresses the crystallization capability, giving rise to an amorphous material with high clearness and toughness. According to previous determination by Differential Scanning Calorimetry at 20°C/min, its glass transition temperature (T_g) was about 82.8°C, and had a sub-T_g (β transition) at about −70°C, as have been revealed after a Dynamic Thermal Mechanic Analysis conducted at 2°C/min and 1 Hz. This second transition has been proposed as the main reason of its ductile behavior at 21°C.

Spectar 14471 was supplied as pellets and extruded sheets of several thicknesses: 1.5, 3.0, 5.0, 8.0, and 10.0 mm. From these sheets, squared tests specimen (25 mm by side) were cut and used for the indentation tests. From the pellets, ISO 3167 dumbbell tensile specimens were injection molded and tested in a universal testing machine (*SUN2500, Galdabini*) equipped with a videoextensometer (*MINTRON OS-65D*) at 21°C and a crosshead rate of 1 mm/min. The engineering stress–strain curve revealed the typical ductile behavior with a yield stress (σ_y) of 49.5 MPa, a Young's Modulus (E) of 2.1 GPa, and a Poisson's ratio (ν) of 0.32, all of them obtained as the mean value of five valid tests.

Impact Indentation Testing

The impact indentation tests were carried out on the instrumented vertical drop weight testing machine *CEAST Dartvis* at 21°C. The dart head tip was hemispherical and made of hardened steel. The specimens were freely supported onto a thick steel plate. A transverse collision took place between the hemispherical tip and the specimen. The small size of the test specimens was selected to obtain a perfect contact between them and the thick steel support plate, which leaded to a very smooth contact curve.

Table I. Geometry Variables Considered in the Study

Geometrical variable	Specimen thickness (mm)	Drop mass (kg)	Indenter diameter (mm)
Thickness	1.5	0.743	12.7
	3		
	5		
	8		
	10		
Drop mass	10	0.743	12.7
		1.043	
		1.343	
Indenter diameter	8	0.743	12.7
		0.764	20

To measure the impact force, a strain-gauge force transducer with a working range of 3.2 kN was mounted on the head tip. The signal was processed by a *CEAST DAS 4000* advanced data acquisition system with a frequency of 500 kHz and stored on a personal computer, and the values of force and time were recorded. No filtering was applied on these recorded values.

The impact energy could be modified by either a change in the drop height (h) or in the drop mass (m). The indenter velocity just before the collision, v_0, could be calculated from the drop height and the gravity acceleration (g). The analysis of the registered contact force versus time curve, $F(t)$, is made from the basis of Newton's second law, and the velocity (v) and the depth of penetration (α) can be obtained[8]:

$$v(t) = v_0 - \int_0^t \frac{F(t) - mg}{m}\,dt \tag{1}$$

$$\alpha(t) = v_0 t - \frac{1}{m}\int_0^t \int_0^t F(t)dt^2 + \frac{1}{2}gt^2 \tag{2}$$

The geometrical parameters defined in a test were the specimen thickness, the hemispherical tip diameter and the drop mass. Keeping these geometrical parameters as constant values, several series of tests were conducted at 21°C, increasing the drop height successively until the registered maximum contact force reached a value of 3200 N. Table I displays the geometrical specifications of the test series carried out.

Restitution Coefficient

The restitution coefficient, ε, is an empirical parameter used to measure the energy dissipated, E_{dis}, during a collision:

$$E_{dis} = \frac{1}{2}mv_0^2(1 - \varepsilon^2) \tag{3}$$

It is defined as the ratio between the indenter velocities, v_1 just after the collision and v_0 just before the collision.

$$\varepsilon = \frac{v_1}{v_0} \tag{4}$$

The restitution coefficient can also be found from an impulse-momentum balance,[9] where t_c is the contact time or the time when the force has just returned to a zero value.

$$\varepsilon = \frac{\int_0^{t_c} F \cdot dt}{m v_0} - 1 \tag{5}$$

The restitution coefficient can also be extracted by another way, provided that it is allowed that the hemispherical tip has a second contact with the specimen:

$$v_1 = \frac{g}{2} t_{nc} \tag{6}$$

where t_{nc} is the noncontact time, that is, the gap between the end of the first collision and the beginning of the second one. The noncontact time can be experimentally measured on the registered force versus time curves.

APPROACH MODELS

The general theory for the contact of two isotropic, perfectly linear elastic spheres is due to Hertz.[7] Results obtained by Rayleigh[1] showed that if the contact duration is very long in comparison with their natural periods, the vibrations of the system can be neglected. It can therefore be assumed that the Hertz law established for static conditions also applies during impact.

The contact between a sphere and a semi-infinite flat plate is a special case in which the radius of one sphere is infinite. In this case, the relation between the contact force and the indenter depth of penetration (α) can be expressed as:

$$F = k\alpha^{3/2} \tag{7}$$

$$k = \frac{4}{3} R^{1/2} \left(\frac{1 - v_1^2}{E_1} + \frac{1 - v_2^2}{E_2} \right)^{-1} \tag{8}$$

where the subscripts 1 and 2 account for indenter and target, respectively, R is the radius of indenter, v is the Poisson's ratio, and E is the Young's modulus. It is assumed that the contact area is small compared to the radius of the indenter and the dimensions of the bodies. Hertz's law should be carefully used on materials with large elastic strains, such as rubber.

The transversal collision between the rigid hemispherical element and the isotropic semi-infinite flat plate of linear elastic behavior could be modeled by the mass-spring system shown in Figure 1(a). In this conservative model, the specimen is replaced by a nonlinear spring of constant k (indentation stiffness), and m represents the drop mass. The equation of the system motion is:

$$m\ddot{\alpha} + mg = -k\alpha^{3/2} \tag{9}$$

The solutions of eq. (9),[5] if the gravity term is not considered, for the maximum penetration (α_m), contact time and contact force (F_M) are:

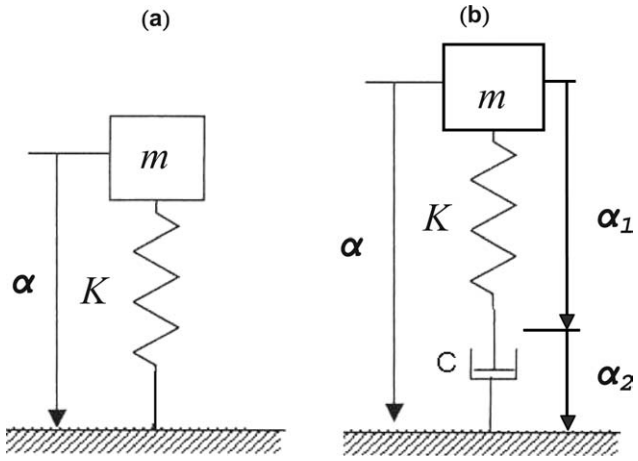

Figure 1. Models (a) conservative and (b) nonconservative.

$$\alpha_m = \left(\frac{5 v_0 m}{4k} \right)^{2/5} \tag{10}$$

$$t_c = 2.94 \frac{\alpha_m}{v_0} \tag{11}$$

$$F_M = k\alpha_m^{3/2} \tag{12}$$

This mass-spring model is a conservative system with analytical solutions. The model does not take energy loss into account. However the model, is valuable for indicating the key variables involved. By one hand, the heavier drop mass, the higher maximum depth of penetration, the higher maximum force and the longer contact time. By other hand, the higher drop height, the greater initial velocity, maximum depth penetration, maximum force, but shorter contact time.

Despite this, almost all real systems are not conservative in a greater or lesser degree. Thus, a better approach is expected by means of a nonconservative system. With this aim a dashpot can be introduced into the conservative system resulting in two different damped mass-spring models; a model where the dashpot is in parallel with the spring, and another where the dashpot is in series.

Although the parallel model accounts for inherent material damping such a hysteretic loss, it does not enable consideration of permanent deformations, which can be addressed by the series model and can be observed on the specimen surface. This viscoplastic model, takes into consideration the permanent deformations that may be observed on the specimen surface.

This series or viscoplastic model is shown schematically in Figure 1(b). The equations of the motion are:

$$m\ddot{\alpha} + mg = -k\alpha_1^{3/2} = -C\dot{\alpha}_2 \tag{13}$$

$$\alpha = \alpha_1 + \alpha_2 \tag{14}$$

where α, α_1, and α_2 are the global, spring, and dashpot displacements, and C is the damping constant. The global depth of penetration is the addition of the elastic (spring) depth of penetration and the plastic (dashpot) depth of penetration. When C is longer the system comes out conservative.

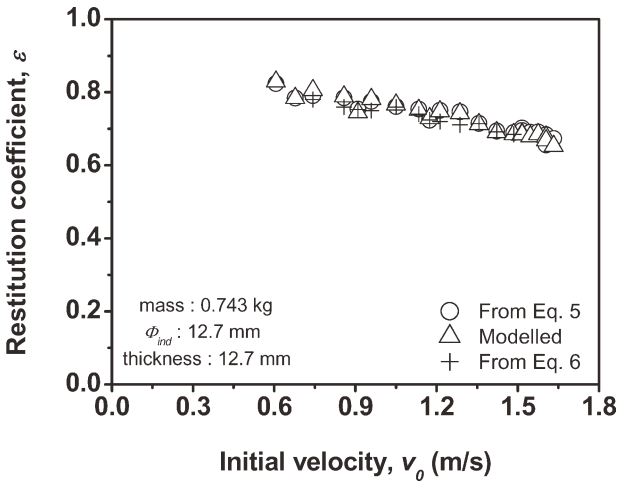

Figure 2. Variation of the restitution coefficient (ε) with initial velocity (v_o) for the test configuration described.

These equations of motion of the nonconservative series model do not have analytical solutions but can be solved using a fourth-order Runge–Kutta numerical integration scheme with a time step shorter than the natural vibration frequency.

Thus, introducing appropriate values of E and C, it is possible to solve the model obtaining the contact force and the depth of penetration, both as a function of the collision time. From the modeled contact force curve, the restitution coefficient may also be calculated through Eq. (5) and compared with the experimental one.

RESULTS AND DISCUSSION

Initial Velocity

The first dynamic indentation tests were performed on the 10-mm thick specimens, using the drop mass of 0.743 kg and the hemispherical head tip of 12.7 mm diameter. The restitution coefficients calculated from the experimental curves by the two methods [eqs. (5) and (6)] had practically the same values and gradually fell with the increasing initial velocity (Figure 2). The values of the restitution coefficients displayed that there was energy loss.

Figure 3(a) shows as solid line the contact forces experimentally recorded for different initial velocities of impact. The registered contact force values were not filtered neither mechanically nor electronically. No dynamic effects can be observed when there is a good contact between the specimen and the thick steel plate and also because the impact velocities are relatively low. In contrast with impact tests with prismatic bars or plates, the specimens in these tests are not accelerated and they are all the time in contact with the support and the striker. As the v_0 values increased, the maximum force grew, and it was found a slight reduction of the contact time as predicted by the conservative model.

The head tip displacement or depth of penetration calculated from eq. (2) are displayed as a continuous line in Figure 3(b), noticing also the residual deformations (α_r). The maximum value of depth of penetration and the residual deformations are displayed in Figure 4. The maximum depth of penetration and the permanent deformations increased (Figure 4), whereas the restitution coefficient gradually fell (Figure 2) with increasing the initial velocity. As initial velocity increased, the indenter had more available energy and the maximum contact force rose, resulting in an increased plastic deformation. As a consequence, the restitution coefficient dropped and the permanent deformation increased because it is related to the energy dissipated.

Thus, to take into account the energy losses indicated by the relatively low values of the restitution coefficient, and the resulting permanent deformations that cannot be predicted by the conservative model, a better approach could be found with a nonconservative series model.

To solve the model the values of E and C must be included, getting the values of contact force and depth of penetration as a function of time and also the restitution coefficient of the modeled contact force versus time curve. The values of E and C were varied until the best fitting with the experimental results was achieved. The conservative model helped us to the fitting, because when E is increased, the contact force also gets larger and the contact time gets shorter. By other hand, in the nonconservative model, the diminution of C leads to smaller values

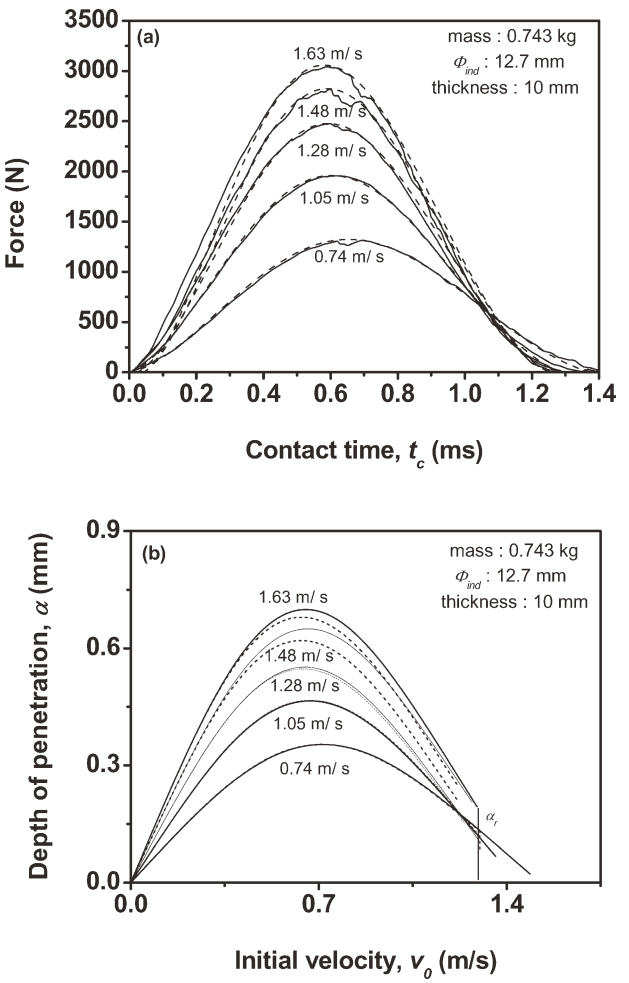

Figure 3. Experimental and modeled traces for (a) contact force (F) versus contact time (t) and (b) penetration (α) versus t plots for the test configuration described.

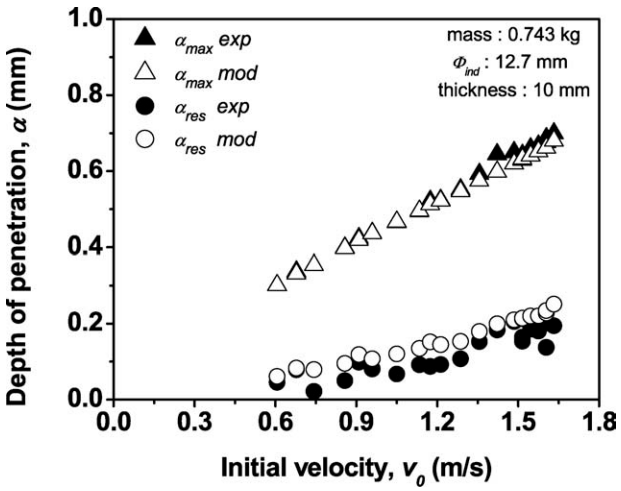

Figure 4. Evolution with initial velocity of the maximum and permanent (residual) penetration determined from the experimental and modeled *F* versus *t* traces, for the test configuration described.

of the restitution coefficient, and the curve force versus time is more asymmetric. The modeled contact forces are displayed as discontinuous lines in Figure 3(a). The modeled depth of penetration is represented as discontinuous traces in Figure 3(b). Both parameters fitted fairly well with the experimental results.

The restitution coefficients of the modeled contact forces were calculated through eq. (9) and represented as hollow triangles in Figure 2. A good fitting was found of the modelled values with the experimental ones. The assessed Young's modulus are represented in Figure 5, which grew slightly as expected with the increase of the initial velocity, as a consequence of the viscoelastic nature of the material. This explains that in the impact tests, the elastic modulus is only a little higher that the tensile tests at low speeds.

The specimens showed a residual impression on the contact surface after the impact tests, as a result of the plastic and viscoelastic deformation. Several residual impressions were analyzed

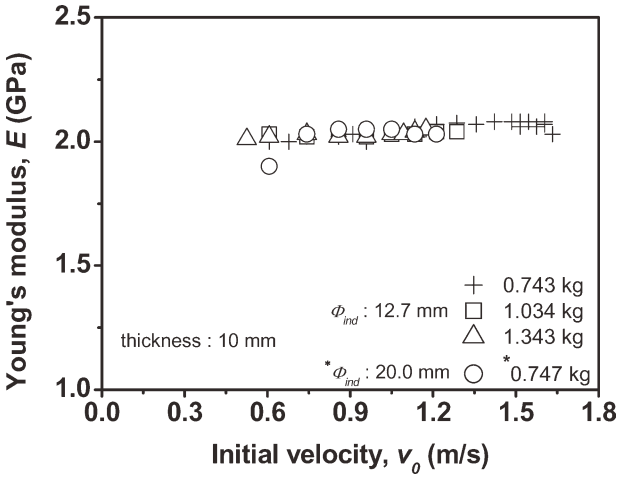

Figure 5. Effect of drop mass on the assessed Young's Modulus at several initial velocities for the test configuration described.

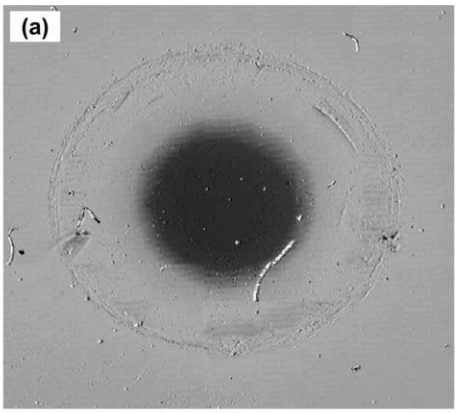

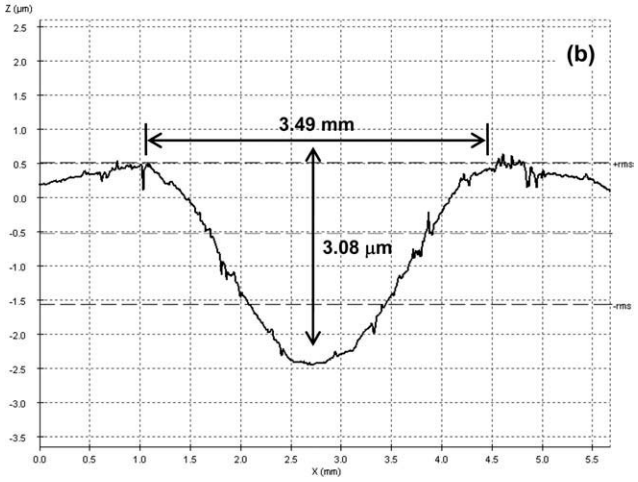

Figure 6. (a) Topography and (b) profiler measurements of the residual imprints for tests carried out at the following conditions: v_0 = 1.63 m/s, mass = 0.743 kg, Φ_{ind} = 12.7 mm, and thickness = 10 mm.

on a scanning confocal microscope (*SENSOFAR*), obtaining a topography of the deformed surface and the diametral profile shape features, showed in Figure 6, at v_0 = 1.63 m/s. The topography of the deformed surfaces had an axial symmetry, without any crack, and the measured dimensions of the imprints are represented in Table II, along with the values of the residual depth of penetration obtained from the model, as well as its related diameters.

The measured imprint diameters agreed very well with the diameters approached by the model. However, the measured depths from the profiler were significantly lower than the values obtained from the model. This reduction may be attributed to the viscoelastic recovery of the material in due course. As far as recovery is concerned, it is greater in depth than in diameter. It has to be pointed out that the determination of the imprint diametrical profile was always carried out 24 h after the indentation test.

The penetration was calculated by the model as the addition of the spring and dashpot displacement. These three displacements are represented in Figure 7 along with the contact force. The spring deformation was elastic and totally recoverable, its maximum took place before the maximum contact force. The

Table II. Estimated (From F–t Experimental and Modeled Traces) and Measured (From Profiler) Imprint Depths and Diameters on the Sample Surface for Several Initial Velocities

	Residual depth		Imprint diameter	
v_0 (m/s)	Model (mm)	Profiler (μm)	Model (mm)	Profiler (mm)
1.52	0.214	1.77	3.30	3.22
1.55	0.220	1.92	3.34	3.39
1.60	0.235	2.64	3.45	3.26
1.63	0.251	3.08	3.57	3.49

Test geometry was: mass drop = 0.743 kg, Φ_{ind} = 12.7 mm, and thickness = 10 mm.

dashpot deformation was not recoverable and increases gradually just to the permanent deformation, α_r, when the collision finished and the force was zero. The addition of these two deformations gives the indenter penetration which had its maximum, α_m, after the maximum force. The indenter returned just begins after the maximum indenter penetration, and was not only elastic and recoverable.

Specimen Thickness

As mentioned before, the series model is based on the Hertz law which was developed for an infinite halfspace. To study the influence of the finite specimen thickness, 1.5-, 3-, 5-, and 8-mm thick specimens, were tested, in addition to the 10-mm thick specimens previously tested. The 0.743 kg drop mass and the 12.7 mm diametrical hemispherical tip were kept.

The 8- and 10-mm thick specimens had the same experimental contact force curves for equal initial velocities, giving identical results. There was no influence of the specimen finite thickness at the used test parameters. This was not the case for the specimens with smaller thickness in which the same test parameters were affected by the steel plate support and thus the model could not be applied. However, for each evaluated specimen

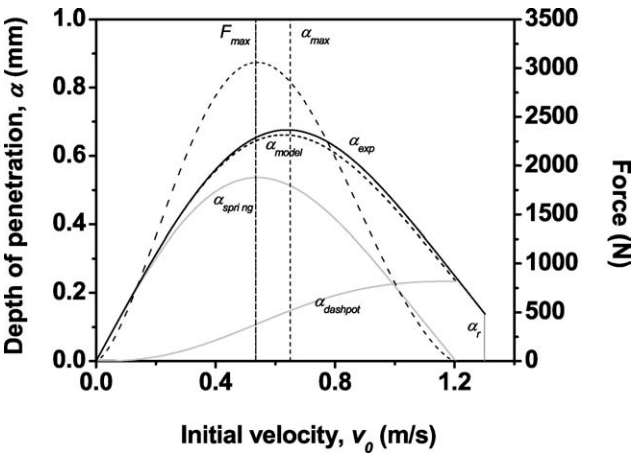

Figure 7. Evolution with the initial velocity of the contact force, global depth of penetration, spring, and dashpot contributions. Testing configuration: v_0 = 1.63 m/s, mass = 0.743 kg, Φ_{ind} = 12.7 mm, and thickness = 10 mm.

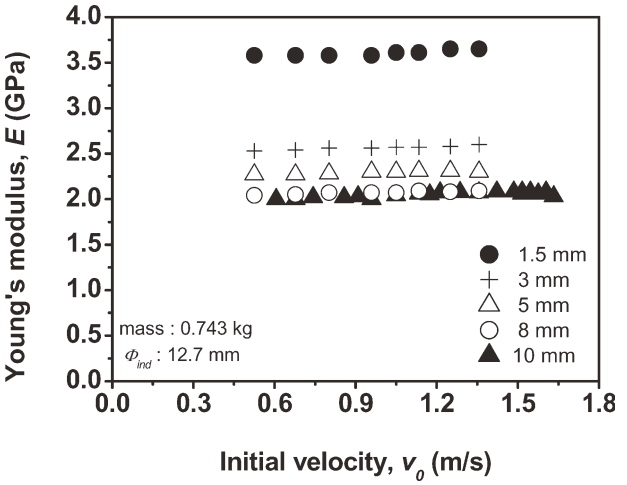

Figure 8. Effect of sample thickness on the assessed Young's Modulus at several initial velocities for the test consideration described.

thickness, the experimental results followed the general trends shown by the 10-mm thick specimens with the initial velocity.

At the same initial velocity but reducing the thickness under a limiting value, the maximum contact force increased, but contact time, maximum penetration and experimental restitution coefficient decreased and the residual deformation got higher.

All the modeled contact force and depth of penetration curves fitted quite well with the experimental ones, including the 5-, 3-, and 1.5-mm thick specimens that were affected by the small thickness. The fitted Young's modulus, represented in Figure 8, were affected, as expected, in the 1.5-, 3-, and 5-mm thick specimen.

When the specimens exceeded a limiting thickness, identical experimental results were obtained, there were no thickness effects and the specimen could be considered as an infinite half space, then to be sure that the contact force was not affected by the specimen finite thickness, it was necessary to test specimens with increasing thicknesses just to obtain the same registered contact force curve.

The tests carried out over two overlapped 5-mm thick specimens showed practically the same experimental results as those obtained with the 10-mm thick specimens, as shown in Figure 9. Thus, piling specimens may be a suitable alternative in case that appropriate thicknesses are not available.

Drop Mass

Whereas the first dynamic indentation tests were performed with a drop mass of 0.743 kg, two new series of tests were performed with 1.043 and 1.343 kg, keeping the same 10 mm specimen thickness and the 12.7 mm diametrical hemispherical tip.

The evolution with the initial velocity of each series followed the same general trends shown in the first series performed with the 0.743 kg drop mass previously analyzed.

For a set velocity, increasing the drop mass, it was observed on the experimental contact force and penetration curves that the maximum force, the contact time and the maximum depth of

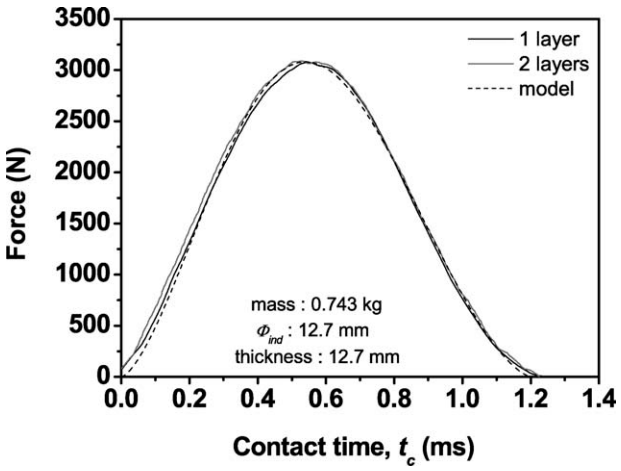

Figure 9. Experimental contact force (F) versus contact time (t) traces for 10-mm thick and overlapped (2 mm × 5 mm) samples. Testing configuration: v_0 = 1.63 m/s, mass = 0.743 kg, and Φ_{ind} = 12.7 mm.

penetration grew, as they can be qualitatively predicted by the conservative model. However, the experimental restitution coefficients were practically identical. The Young's modulus resulting of the fittings are represented in Figure 5. Their values were independent on the drop mass and only varied slightly with the initial velocity.

Head Tip Diameter

To analyze the effect of the hemispherical tip diameter, a 20-mm diametrical hardened steel hemisphere was employed. A series of tests were performed with this modified indenter on specimens with a thickness of 8 mm. These new series of tests can be compared with the previously analyzed tests series which had the same specimen thickness, the 12.7 mm diametrical hemispherical tip and a drop mass of 0.743 kg.

The evolution of the experimental contact force, penetration and restitution coefficients with increasing initial velocities followed the general trends shown by the previously analyzed series. The larger hemispherical tip diameter resulted in a greater maximum contact force, and lower values of the maximum penetration. The restitution coefficient was also reduced and consequently the permanent deformation increased.

The values of the resulting Young's modulus of the best fitting between the experimental and modeled curves are represented in Figure 5. The Young's modulus values of the 20 and 12.7 mm indenter diameter series of tests were the same.

Young's Modulus

A consistent model could satisfy the criteria of independence of the geometrical parameters. The Young's modulus is a material property that only may vary with the strain rate at constant temperature.

In Figure 5, it can be observed that the assessed modulus by the model were independent on both the drop mass and the indenter diameter, whereas in Figure 8, the values were also the same when the specimen satisfied the thickness criteria previously explained. In addition, the modulus values slightly increased, as expected for the viscoelastic nature of the polymer, with the initial velocity (strain rate).

CONCLUSIONS

The restitution coefficients calculated by two independent methods give the same values. It is clear from this analysis that the coefficient of restitution is not a material property, its value varies with the initial velocity and the head tip diameter. At sufficient low velocities the restitution coefficient approaches to unity but gradually falls with increasing velocity; this is the reason why the conservative model does not match with the experimental results.

The series or viscoplastic model is a very good approach to the PETG behavior during the dynamic indentation. There is a very good fitting with the contact force, depth of penetration, and restitution coefficient. In addition, there is also an agreement with the permanent deformations shown by the PETG, which deforms plastically.

The nonconservative model satisfies the criteria of independence of geometrical parameters; only the specimen thickness can violate the infinite thickness hypothesis. However, it is easy to check the specimen thickness influence, by testing pilled specimens.

The application of this methodology allows to assess the Young's modulus at high strain rates, and the calculated value does not depend on the drop mass and head tip diameter, but rises slightly with increasing initial velocity (strain rate), as it is expected of the viscoelastic nature of the PETG.

ACKNOWLEDGMENTS

The authors would like to acknowledge the financial support provided by the Subdirecciœn General de Proyectos del Ministerio de Educación y Ciencia (Government of Spain) through the project MAT2009-14294.

REFERENCES

1. Timoshenko, S. P.; Goodier, J. N. Theory of Elasticity, 3rd ed.; McGraw-Hill: Singapore, **1982.**
2. Sánchez-Soto, M.; Martinez, A.-B.; Santana, O. O.; Gordillo, A. J. *Appl. Polym. Sci.* **2004,** *93*, 1271.
3. Southern, E.; Thomas, A. G. *J. Appl. Polym. Sci.* **1972,** *16*, 1641.
4. Vriend, N. M.; Kren, A. P. *Polym. Test.* **2004,** *23*, 369.
5. Zukas, J. A.; Nicholas, T.; Swift, H. F.; Greszczuk, L. B.; Curran, D. R. Impact Dynamics; Krieger Pub. Co.: Malabar, **1992.**
6. Rydin, R. W.; Karbhari, V. M. *Int. J. Impact Eng.* **1998,** *21*, 773.
7. Johnson, K. L. Contact Mechanics; Cambridge University Press: Cambridge, **1985.**
8. ISO 6603-2. Plastics—determination of puncture impact behaviour of rigid plastics—part 2: instrumented impact testing.
9. Jiménez, O.; Sulcahuamán, J. A.; Sánchez-Soto, M.; Martínez, A. B. *Int. J. Solids Struct.* **2005,** *42*, 5758.